Electrochemical and density functional theory studies of some newly synthesized azo-stilbene chromogenic structures

Liviu V. Costea[1] ● Maria-Elena Rădulescu-Grad[2] ● Günter Fafilek[3]

Received: ……/Accepted …

Abstract The electrochemical behavior in nonaqueous media of a series of five newly synthesized azostilbene dyes is investigated with the aim of elucidating the anodic oxidation mechanism of the latter to gain a better understanding of potential oxidative degradation phenomena in order to find new and environmentally sustainable electrochemical methods for the abatement of dyes from industrial wastewater. In addition, the frontier orbital energies of optimized conformers have been computed using quantum chemical calculations at the B3LYP-D3 (dispersion corrected Becke, 3 parameter, Lee Yang Parr) level of theory. Cyclic voltammetry experiments show that anodic oxidation of the studied chromophore structures follows an irreversible pathway and most probably occurs at the amide nitrogen. Validation of experimental results has been conducted by computation of various global reactivity descriptors, confirming that substituents grafted on the benzene ring actively influence the oxidation/reduction potentials.

Keywords Azostilbene Dyes ● Density functional theory ● Electrochemistry ● Molecular modelling ● Voltammetry

(Four to six keywords, at least three should be taken from the keyword listing available at the Springer web page: http://www.springer.com/chemistry/journal/706 → Instructions for authors → Keyword list for authors). The keywords should characterize the scope of the paper, the principal materials, and main subjects. Do not duplicate words already contained in the title!

✉ Liviu V. Costea

livius.costea@gmail.com

[1] University "Politehnica" Timişoara, Faculty of Industrial Chemistry and Environmental Engineering, 300223 Timişoara, Romania.

[2] "Coriolan Drăgulescu" Institute of Chemistry, Romanian Academy, Mihai Viteazu Blvd. No. 24, 300223 Timisoara, Romania.

[3] Institute of Chemical Technologies and Analytics, Technische Universität Wien, 1060 Vienna, Austria.

Introduction

Azo dyes, representing the largest cluster of synthetic colorants, account for about 60 % of the known commercial dyes as well as for 70% of all the chromogenic structures synthesized worldwide [1, 2]. Azo-stilbene dyes represent a subdivision of the class of azo dyes, being prepared by means of the classical azo-coupling reaction starting from 4,4′-diamino-2,2′-stilbenedisulfonic acid [3]. Considering that about 70 % of all industrially useful chromogenic structures are azo derivatives [4] it is no surprise that their field of application expands to numerous other domains like food industry, pharmaceutical, cosmetic, textile, and leather industries, printing, optical materials, medicine etc. [5-9]. Some of the most significant examples regarding the wide range of applications that characterizes this category of dyes are mainly: optical materials [10], antiviral agents [11] and in various dyeing processes of cellulosic fibers [12], with a special emphasis on those with fluorescent properties. This class of dyes is also being investigated in connection to its potential use in organic light emitting diodes (OLEDs) [13, 14] etc. To our knowledge so far, bibliographical data related to the electrochemical behavior of dyes based upon the azo stilbene scaffold is quite limited.

In this regard, we have investigated a series of azo stilbene dyes obtained, using acetoacetanilides substituted at the aromatic ring as coupling

components [15], by means of cyclic voltammetry in nonaqueous solvents as well as quantum chemical calculations.

Electroanalytical techniques, with their purposeful approach and substrate specific acuity towards the investigated processes make them attractive alternatives to other analytical methods [16 - 18]. Electrochemical analysis and syntheses of organic compounds has gained momentum in the last decade, mostly because of its environmentally benign approach, the cost effectiveness and its enhanced process safety [19]. Variously modified anodes have successfully been employed in numerous attempts towards electrochemical degradation and discoloration of azo dyes in the effort of developing more efficient industrial wastewater treatment methods [20 - 22].

Cyclic Voltammetry, a well-known versatile and effective electroanalytical technique has been employed to shed light mostly upon qualitative aspects of charge transfer phenomena [23]. As a valuable tool, voltammetry has often been used in the study of mechanistic as well as kinetic aspects of electrode processes involving organic dyes [2, 16]. Our previous findings regarding the electrochemical behavior of variously substituted nitrogen heterocycles [24, 25] showed that cyclic voltammetry can be successfully employed in elucidating charge transfer mechanisms involving complex organic structures.

Based on our earlier work in investigating electrode processes of organic substrates, we herein report the electrochemical and computational study of a series of five newly synthesized azo-stilbene chromogenic structures as described in Scheme 1. The latter dyes have been investigated using cyclic voltammetry in nonaqueous media as well as by calculating various quantum chemical parameters, to elucidate the mechanisms that could cause color fading due to various oxidative processes occurring within the substrate molecule as well as potential new methods of abatement of synthetic colorants from certain eluents [21, 26]. Since the electrode potentials at which oxidation and reduction of organic compounds takes place largely rely on substrate molecular geometry as well as spin density distribution, appropriate computational models must be employed for a comprehensive understanding of the electrochemical processes that they undergo [27]. Quantum chemical methods, like the Density Functional Theory (DFT) are indispensable means that, complementary to experimental results, contribute to elucidating the voltammetric behavior of organic substrates [28].

Scheme 1

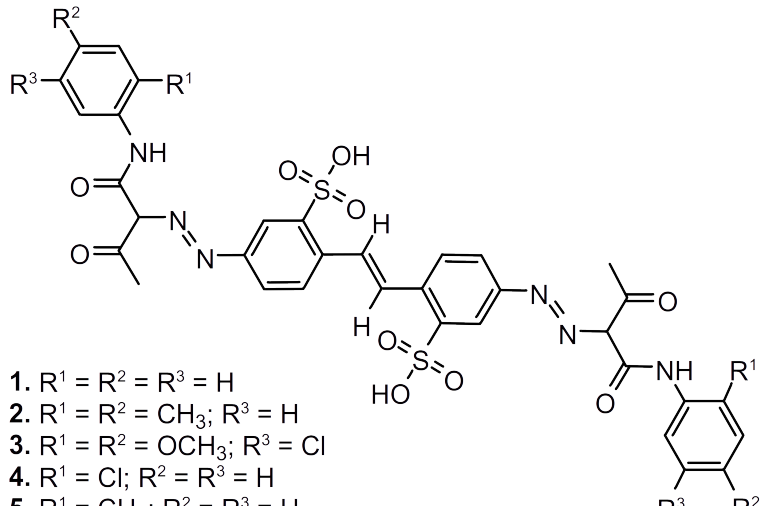

Results and Discussion

Electrochemical behavior

Compared to other methods currently in use, anodic oxidation of chromogenic substrates, leading to easily removable and/or biodegradable compounds, has attracted many research teams around the world [26, 29]. In this respect, assessment of redox stability of organic dyes and investigation of possible oxidation pathways is of paramount importance.

The stability towards oxidation/reduction of five variously substituted derivatives of 4,4'-diaminostilbene-2,2'-disulfonic acid (compounds 1 - 5, Scheme 1) has been investigated by cyclic voltammetry in deoxygenated nonaqueous DMSO with the aim of revealing the specific oxidation pathways and mechanisms leading to the specific degradation products.

Figure 1 presents the typical current-voltage diagrams of the stilbene dyes recorded in anhydrous, deoxygenated DMSO using Pt working and counter electrodes.

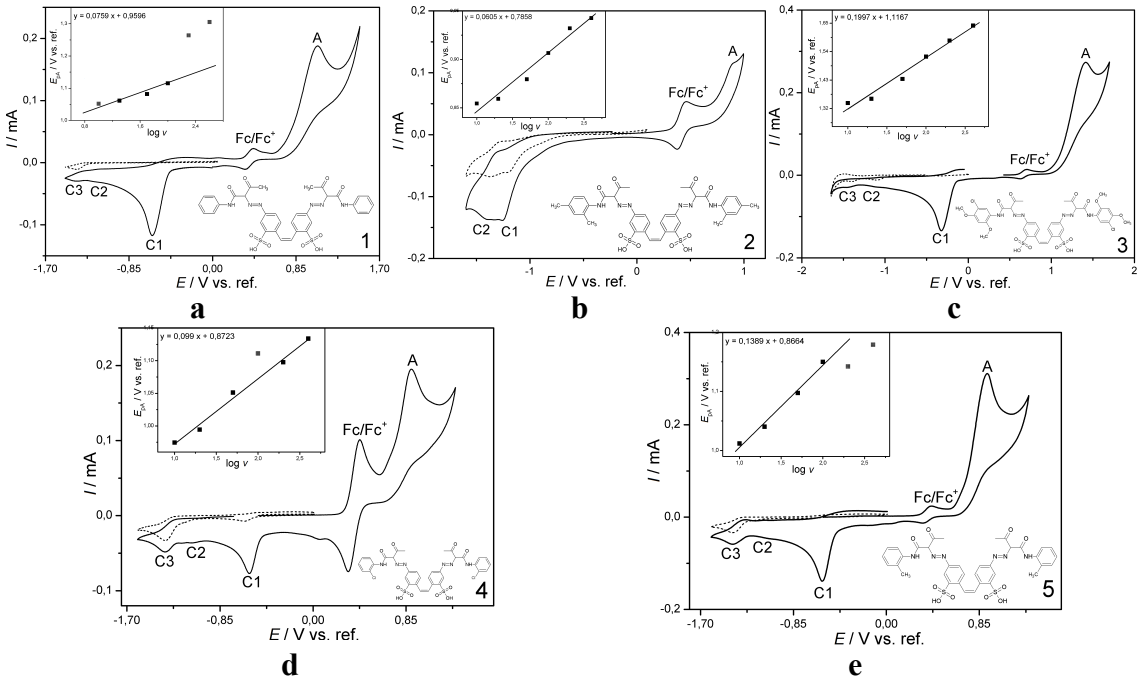

Fig. 1 Cyclic voltammograms of compounds **1** - **5**. Conditions: substrate concentration, c=2·10^{-3} mol·dm^{-3}; scan rate 50·10^{-3} V·s^{-1}. Dotted line: Cyclic voltammogram of **1** - **5** cathodic scan, recorded in the same conditions. Inset: variation of oxidation peak potential with logarithm of scan rate.

While varying the electrode potential towards positive values, one well-defined oxidation peak (*A*) appears on all voltammograms at potentials between 0.5 V (compound **2**, Scheme 1) and 7.5 V (compound **3**, Scheme 1). No other oxidation waves occur within the studied potential range. Reversing the scan direction reveals a sharp, pronounced reduction peak (*C*1) occurring

at potentials ranging from E_{C1}= -0.96 V (compound **5**, Scheme 1) and -1.73 V (compound **3**). A second, less delimited reduction wave (*C*2) of smaller height and significantly broader shape occurs at potentials between E_{C2}= -1.44 V (compound **5**) and 1.81 V (compound **3**). A third, weaker, but well-defined cathodic peak (*C*3) occurring at potentials between -1.73 V (compound **4**, Scheme 1) and -2.14 V (compound **3**) is characteristic for all studied dyes. Although, while scanning over the full potential scale of the electrochemical window reveals all signals reported above, sweeping the potential cathodically, starting from the open circuit potential (OCP), remarkably reveals only the last two reduction peaks *C*2 and *C*3 (**Fig. 1** dotted line).

Considering the shape of the voltammograms of substrates **1** - **5** (Scheme 1) with respect to the single anodic wave (*A*) (**Fig. 1**) and bearing in mind that the cathodic scans give rise of only two well defined reduction signals, one can assume that peak *C*1 occurs as a direct consequence of the previous anodic oxidation of the investigated dyes. This behavior is a common feature for all derivatives except for compound **2**, which is the only structure in the studied series lacking this specific signal.

The anodic signal (*A*) observed in all investigated compounds as well as the lack of any coupled reduction peak within the anodic potential window is the most obvious criterion for its electrochemical irreversibility. This

behavior can come because of two types of mechanisms, namely: a relatively fast succeeding homogenous reaction preceded by the loss of an electron [30], or a high kinetic barrier of the heterogeneous electron transfer resulting in a sluggish electron release step [31]. The latter option would be thus characterized by a small heterogeneous charge transfer rate on the timescale of the experiment, relative to the rate of diffusion.

Investigation of surface phenomena

To undertake a preliminary assessment on the prospect of the surface phenomena mentioned above, multi-cyclic scans of the studied compounds have been recorded, a representative example being shown in Fig. 2. As can be seen, the height of the oxidation peak *A* regresses with a small amount on every successive scan upon cycling multiple times at the same sweep rate. This behavior often relies on electrode fouling or upon adsorption [32].

Electroactive materials, such as organic molecules, reaction intermediates or products of the ongoing processes can deposit onto the electrode, contaminating its surface thus altering the current - voltage profile [33]. Although in some cases the compounds confined at the metal/solution interface act as mediators, thus enhancing electron transfer, in most instances the adsorbed species simply acts as inhibitors diminishing the heterogeneous charge transfer rate constant [34]. The latter case may cause a certain deviation from linearity of the peak potential dependence on the logarithm of

sweep rate at higher scanning speeds seen in substrates **1**, **4** and **5** (**Fig. 1** Inset).

For an electrochemically irreversible system under pure diffusion control, the Randles-Sevcik equation specifies the voltammetric peak current [35, 36]:

$$i_p = 2,99\times10^5 n(\alpha n_a)^{1/2} A C_\infty D^{1/2} v^{1/2} \quad (1)$$

In this case, i_p corresponds to the peak current density, n denotes moles of electrons exchanged per mol of substrate, α is the charge transfer coefficient, na stands for the stoichiometric number of electrons transferred during the rate determining step, A being the electrode area, C_∞ the substrate concentration at infinite distance (into the bulk solution), D the diffusion coefficient of the electroactive species and v the potential scanning speed. It follows straight forward that an irreversible electrochemical system under diffusion control and no kinetic complications should exhibit a linear variation of i_p relative to $v^{1/2}$ with the origin as the intercept [37].

The inset of Fig. 2 shows that the anodic process of substrate **1** follows the modified Randles-Sevcik equation (Eq. 1). The peak current follows a linear variation with respect to the square root of the sweep rate but clearly deviates from the origin thus reflecting either a certain influence of adsorption or of a coupled chemical reaction on the overall potentiodynamic response [37, 38]. This underpins the irreversibility of the anodic process

associated with peak *A* and on the other hand the predominant diffusion control at lower sweep rates. Deviation from linearity at higher scan rates (i.e., peak heights I_p lower than predicted) is apparent in the I_p vs. $v^{1/2}$ plot. At sweep rates above 0.1 $V \cdot s^{-1}$, the oxidation of the studied compounds occurs at much higher potentials (Fig. 1 a-e Inset) and generates lower peak intensities than predicated by the linear correlation (Fig. 2 Inset)

A plot of log*I* vs. log*v* recorded for the oxidation peak of substrate **1** (Fig. 3 Inset A) renders a straight line with the slope of 0.37, diverging from the theoretical value of 0.5 [39]. This can originate in electrode surface fouling due to specific adsorption of non-electroactive species or to adherent oxidation products formed at the metal/solution interface, impeding the electrode reaction [40]. This leads to smaller charge transfer rates and higher oxidation overpotentials [41].

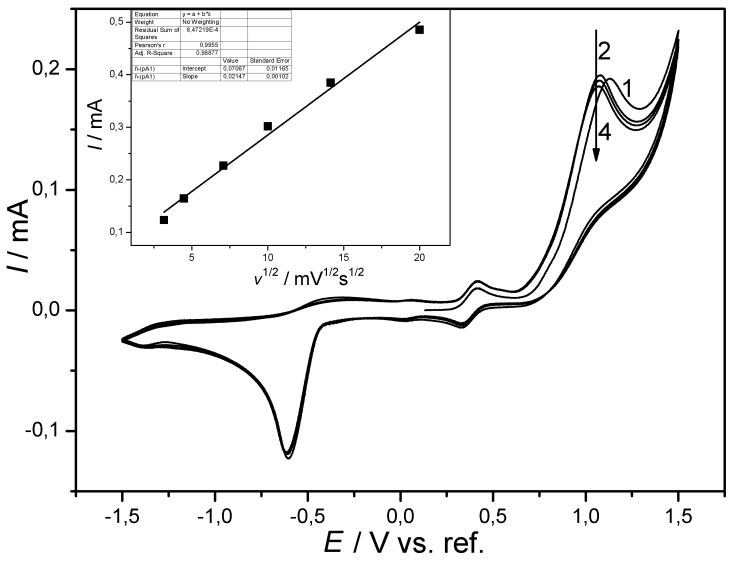

Fig. 2 Cyclic voltammogram of **1** over the entire potential window, 4 cycles. Conditions: substrate concentration, c=2·10^{-3} mol·dm^{-3}; v = 50·10^{-3} V·s^{-1}. Inset: variation of oxidation peak height on square root of the scan rate.

Influence of sweep rate variation

To thoroughly investigate the electrochemical properties of the studied dyes, we further analyzed their anodic oxidation. Appropriate and more detailed information on the parameters playing a role in the overall anodic oxidation process of the investigated dyes, including the charge transfer kinetics can be obtained by recording the cyclic voltammograms of the studied substrates at various sweep rates.

Table 1 Voltammetric data collected for dyes **1** - **5**[a)]

Dye	E_A / V[b)]	E_{C1} / V	E_{C2} / V	E_{C3} / V	$(E_A-E_{A/2})\cdot10^{-3}$/ V	$(\partial E_A/\partial \log v)$ / V
1.	0.696	-0.988	-1.579	-1.742	0.179	0.076
2.	0.491	-1.678	-1.791	--	0.099	0.061
3.	0.749	-0.989	-1.788	-2.136	0.205	0.199
4.	0,677	-0.956	-1.499	-1.727	0.157	0.097
5.	0.725	-0.960	-1.466	-1.778	0.156	0.139

[a)] Conditions: substrate concentration c=2·10^{-3} mol·dm^{-3}; v = 50·10^{-3} V·s^{-1}

[b)] Potentials referred to the Fc/Fc$^+$ redox couple

A set of voltammograms, typical for the entire investigated series, is that of compound **1**, depicted in Fig. 3. It is obtained by polarizing the electrode from the OCP towards more positive values and varying the sweep rate for each scan (between 0.01 and 0.4 $V \cdot s^{-1}$). No reduction signal in the reverse scan is visible, even at very high *v* over this potential range, suggesting a sluggish charge transfer or the occurrence of a coupled chemical reaction [30, 31], rendering the overall process as irreversible.

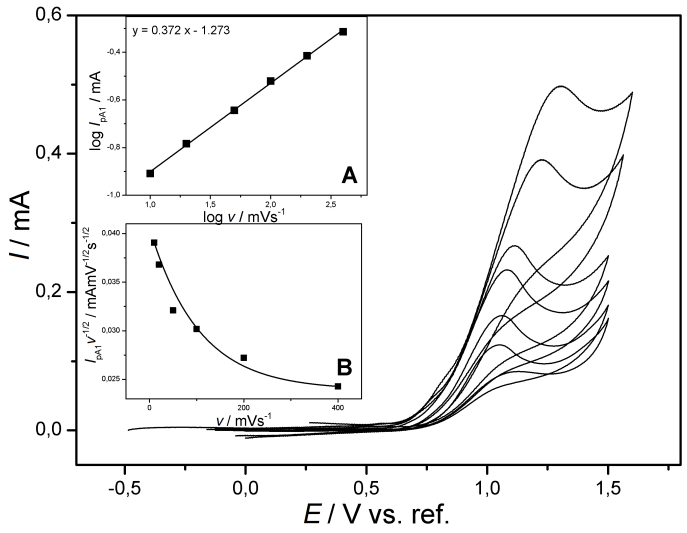

Fig. 3 Cyclic voltammogram of **1**, anodic region. Conditions: substrate concentration, $c=2 \cdot 10^{-3}$ $mol \cdot dm^{-3}$; scan rates 10 - $400 \cdot 10^{-3}$ $V \cdot s^{-1}$ Inset A: Plot of log*I* vs. log*v* for the oxidation peak of substrate **1**. Inset B: Variation of the current function ($I_A \cdot v^{-1/2}$) with *v* for the oxidation peak of substrate **1**

It is noteworthy that, for a totally irreversible anodic oxidation process, the peak potential varies with sweep rate, shifting towards more positive values, by a factor of $30/\alpha$ mV at 25^0C, for a tenfold raise of the scanning speed [33, 42]. All studied compounds account for an anodic signal (A) that shifts towards more positive potentials with increasing v. This common feature, visible in all studied cases, leads to E_A varying linearly with log$v$ (Fig. 1 inset). However, linearity of the peak dependency on v holds, in some cases, only for sweep rates lower than 0.2 $V \cdot s^{-1}$. At higher scanning speeds, the slope changes to greater values, probably due to the increasing influence of adsorption phenomena [43].

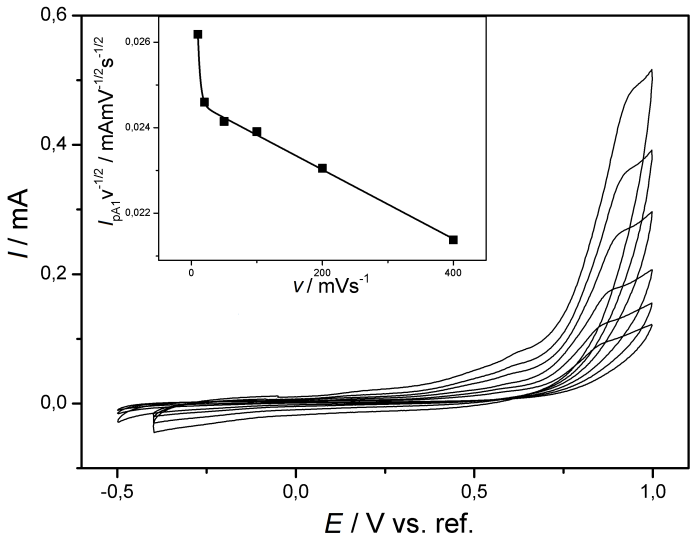

Fig. 4. Cyclic voltammogram of **2** anodic region. Conditions: substrate concentration, c=$2 \cdot 10^{-3}$ $mol \cdot dm^{-3}$; scan rates 0.01 - 0.4$\cdot$ $V \cdot s^{-1}$ Inset: Variation of the current function ($I_A \cdot v^{-1/2}$) with v for the oxidation peak of substrate **2**

Voltammograms of dye **2** drawn by scanning towards positive potentials at various sweep rates are shown in Fig. 4. A single relatively weakly contoured wave can be seen at E_A= 0.87 V vs. ref (v = 0.05 V·s^{-1}), shifting towards more positive values with increasing v. It shows no cathodic counterpart over the given potential window, even at higher scan rates suggesting an irreversible charge transfer process. It is worth mentioning that, although the oxidation of compound **2** occurs at a less positive potential compared to the other studied dyes, its general electrochemical behavior is following the established pattern seen in all investigated substrates (Figure 1). The difference in oxidation potential most probably relies on the electronic effects exerted by the two methyl groups over the reaction center (*vide infra*).

The so-called current function, (*i.e.*, the peak height I_A, normalized with the square root of v) $I_A \cdot v^{-1/2}$ calculated for the oxidation signal of all the studied dyes and plotted against v (Figure 3 inset B, Figure 4 Inset) reveals remarkably similar shapes for all compounds, namely an exponential decay. The latter behavior is suggestive for a slow charge transfer reaction followed by an irreversible homogeneous reaction (EC_{irr} mechanism) [44, 45].

As can be seen in Figure 5, the oxidation peaks get broader with increasing scan rate and the peak potential varies linearly with the logarithm of v (Figure 1 Inset), with slopes ranging between 0.061 and 0.099 V per

tenfold increase in v. Both behaviors suggest that the anodic oxidation of the studied dyes occurs at potentials much higher than the formal potential, *i.e.*, at high overpotentials [46]. Thus, the rate-limiting step probably consists of a slow heterogeneous charge transfer occurring under diffusional control.

Estimation of charge transfer coefficients

The anodic transfer coefficient was determined in order to get more insights on the mechanism of anodic oxidation of the latter dyes, using three separate methods.

Voltammograms on completely irreversible reactions, where the peak is broadening with increasing sweep rate, like the ones investigated herein, are known to be characteristic for slow charge transfer followed by a coupled homogenous reaction [43]. In these cases, *Tafel* analysis could facilitate determining the transfer coefficient for the rate determining step, α_{rd} [47].

In this first approach, a *Tafel* plot (Fig. 5 Inset) was drawn from the anodic response of the studied dyes recorded at a low scan rate (v = 0.01 $V \cdot s^{-1}$). To quantify the influences of heterogeneous charge transfer kinetics more accurately and to avoid the effects of diffusion that are more visible near the peak [48], only the rising part of the peak current was considered.

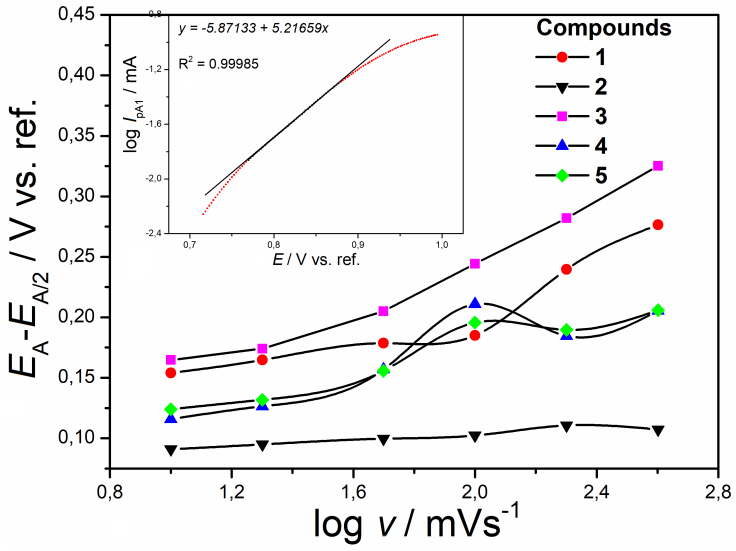

Fig. 5 Variation of E_A-$E_{A/2}$ on the scan rate range 0.01-0.4 V·s^{-1} for compounds **1** - **5**. Inset: *Tafel* plot drawn from the rising part of the current-potential curve of compound **1** recorded at v = 0.01 V s^{-1}

Typical *Tafel* behavior with linear dependence of the logarithm of current on the applied potential is being observed for all studied dyes. For substrate **1** (Scheme 1), for example, it holds for potentials between 0.77 - 0.88 V vs ref. The slope of the latter linear regression can be employed to estimate the value of α_{rd} [49] using the following equation [34]:

$$b = (2.3 \cdot RT)/(\alpha_{rd} \cdot n' \cdot F) \quad (2)$$

where b stands for the *Tafel* slope, R - the universal gas constant, n' the number of electrons exchanged in the rate determining step per substrate molecule. Data for all investigated dyes are listed in Table 2.

Table 2. Anodic transfer coefficient, assumed number of electrons, mean value of ΔE_p

Dye[a)]	α_{rd}[b)]	α_{avg}[c)]	α_{app}[d)]	*n'* (assumed)	$(E_A\text{-}E_{A/2})_{avg}$/ V
1	0.308	0.388	0.283	1	0.199
2	0.276	0.401	0.478	1	0.101
3	0.265	0.188	0.249	1	0.205
4	0.349	0.304	0.332	1	0.167
5	0.366	0.293	0.326	1	0.168

[a)]Conditions: substrate concentration $c=2\cdot10^{-3}$ mol·dm^{-3}, ref. Ag/AgCl

[b)] Data obtained from the *Tafel* plot at $v = 0.01$ V·s^{-1}

[c)] Data obtained from the slope of E_A vs. log$v$; up to $v = 0.1$ V·s^{-1}

[d)] Data obtained using Eq. (4)

Secondly, data shows that for each studied dye, the anodic peak potential (E_A) varies linearly with the logarithm of v. Up to 0.1 V·s^{-1} (Fig. 1 a-e Inset) the slope of the latter dependency is utilized for calculating an average value of the transfer coefficient over a broader range of scan rates, α_{avg} [50]. For the case of an irreversible electrode process, like the ones shown in this work, the linear dependency between the peak potential and sweep rate can be described by Eq. (3) [51].

$$E_A = (b/2) \log v + \text{Cst} \quad (3)$$

The values for α_{avg} presented in Table 2 are in good agreement with those obtained using the first approach.

Thirdly, it has been shown that for irreversible electrochemical signals, like the ones studied herein, the difference between the peak and half-peak potential, $E_{A/2}$ (*i.e.,* the electrode potential recorded at half the peak height) is inversely proportional to the apparent charge transfer coefficient, α_{app} according to Eq. (4) [33, 35, 38].

$$|E_A - E_{A/2}| = 1.857RT/\alpha_{app} \cdot n' \cdot F \quad (4)$$

In the above equation *n'* stands for the number of electrons transferred per substrate molecule during the rate determining step, while *R*, *F* and *T* have their usual meanings. Table 2 shows values for (E_A - $E_{A/2}$), for each substrate averaged over the entire range of sweep rates. The resulting values for α_{app} are consistent with a one-electron transfer per molecule in the first oxidation step of the investigated substrates.

The assumption of a slow heterogeneous charge transfer as the first oxidation step, is further underpinned by the value of the anodic transfer coefficient that is constantly lower than 0.5 (Table 2) suggesting a concerted oxidation pathway governed by charge transfer kinetics [52].

Calculation of frontier orbital (FO) energies, DFT computations

It is known that the redox properties of organic substrates are deeply linked to their electronic structure thus, quantum chemical calculations can offer the necessary background to sustain the results obtained experimentally.

Substituents grafted on the outer benzene ring play a significant role through their electronic effects on the voltammetric response of the mentioned substrates. Compound **2** (Scheme 1), for example, bears two *methyl* groups grafted on the outer benzene ring. While the one in *para* position exerts its resonance electron donor effect (+*M*) through hyper-conjugation, the same group placed in the *ortho* position shows an inductive donor effect (+*I*), leading to an electron-rich amidic nitrogen as the main oxidation site. The same rationale holds for compound **3** (Scheme 1), where the *para methoxy* group as well as the chlorine at the *meta*-position, both showing mesomeric electron donor effects (+*M*), increase the electron density at the carbon atom linked to the amidic nitrogen thus leading to a higher spin density at the latter reaction center. The inductive electron releasing effect of the *methyl* group present in dye **5** (Scheme 1) could favor an extended conjugation in the phenyl-amino-enolic tautomer (Scheme 2). On the other hand, the chlorine atom in dye **4** (Scheme 1), with its strong –*I* effect could favor an internal conjugation between the amino- and the phenyl

groups, hence decreasing electron density as well as the extended conjugation with the azo-stilbene system.

Scheme 2

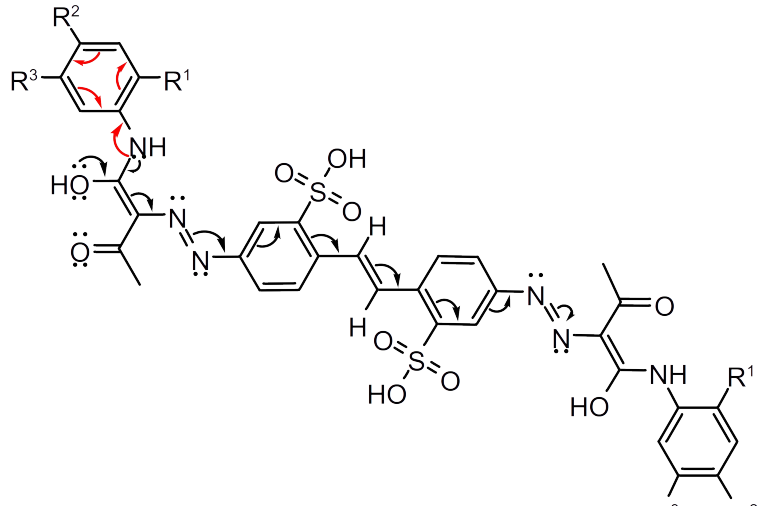

The above presented data, point towards an $EC_{irr}E$ mechanism involving a slow initial one-electron charge transfer step with the formation of a radical cation intermediate, most probably at the amidic nitrogen atom, followed by the deprotonation of the latter and subsequently by a second charge transfer step in which the deprotonated intermediate loses one electron. To further substantiate these findings and to get more detailed information on the charge transfer site of the substrate molecules, computational optimization of the studied structures has been employed and energies of frontier orbitals as well as other reactivity descriptors have been computed.

The ground state geometries of compounds **1 - 5** (Scheme 1) have been preoptimized using the Hartee-Fock method using the 3-21G basis set. Density functional theory (DFT) at the B3LYP-D3 level using the 6-31G* basis set was applied for the final geometry optimization in the gas phase, as well as for the calculation of FO energies, dipole moments and polarizabilities. Solvation energies have not been accounted for since solute-solvent interactions as encountered in the bulk solution do not apply as such to the electrical double layer.

Anodic oxidation of organic substrates occurs by discrete electron release from the highest occupied molecular orbital (HOMO). Thus, in order to investigate possible oxidation sites of the studied chromogenic structures, electron density calculations were performed on the ground state conformers. The optimized structures of the investigated dyes, the localization of spin densities of the HOMO, and the orientation of the molecular dipole moment are presented in Figure 6 and their energy values enlisted in Table 3.

As can be seen, the HOMO orbitals of all the studied diaminostilbene derivatives are delocalized on the outer benzene ring and, more importantly, on the nitrogen atom of the acetamide moiety, making this part of the molecule more susceptible to electron release.

To confirm the calculated values, the FO energy levels for all five substrates have been estimated using information gathered by cyclic voltammetry. The energy of the HOMO was calculated using the potential corresponding to the rising part of the oxidation wave measured at a scan rate of 0.05 $V \cdot s^{-1}$, the so-called onset potential (E_{onset}^{Ox}) [53]. This region is defined as being the potential at which the release of one electron from the molecular HOMO becomes detectable from the rise in anodic current. The inverse rationale involving the onset potential of the reduction wave, E_{onset}^{Red} holds for the acceptance of one electron on the molecular LUMO [54]. The FO energy levels estimated from CV are obtained using equations (5) and (6) considering the formal potential of the Fc/Fc^{+} couple being 5.1 eV on the Fermi scale [55].

$$E_{HOMO} = -(E_{onset}^{Ox} + 5.1) / eV \quad (5)$$

$$E_{LUMO} = -(E_{onset}^{Red} + 5.1) / eV \quad (6)$$

The FO values estimated from CV (Table 3) are in good agreement with those obtained by computational DFT simulations (Figure 6). The observed differences could arise due to experimental conditions, considering that the voltammograms are prone to solvent effects while DFT geometry optimizations have been conducted in the gas phase. The latter finding

underscores the validity of the computed values and the interactions of the grafted substituents with the reaction center. From the values presented in Table 2, one can see that substrate **2**, baring 2, 3-dimethylaniline groups accounts for the highest HOMO energy level, whereas substrate **4**, baring 2-chlorolaniline scaffold shows the lowest energy level.

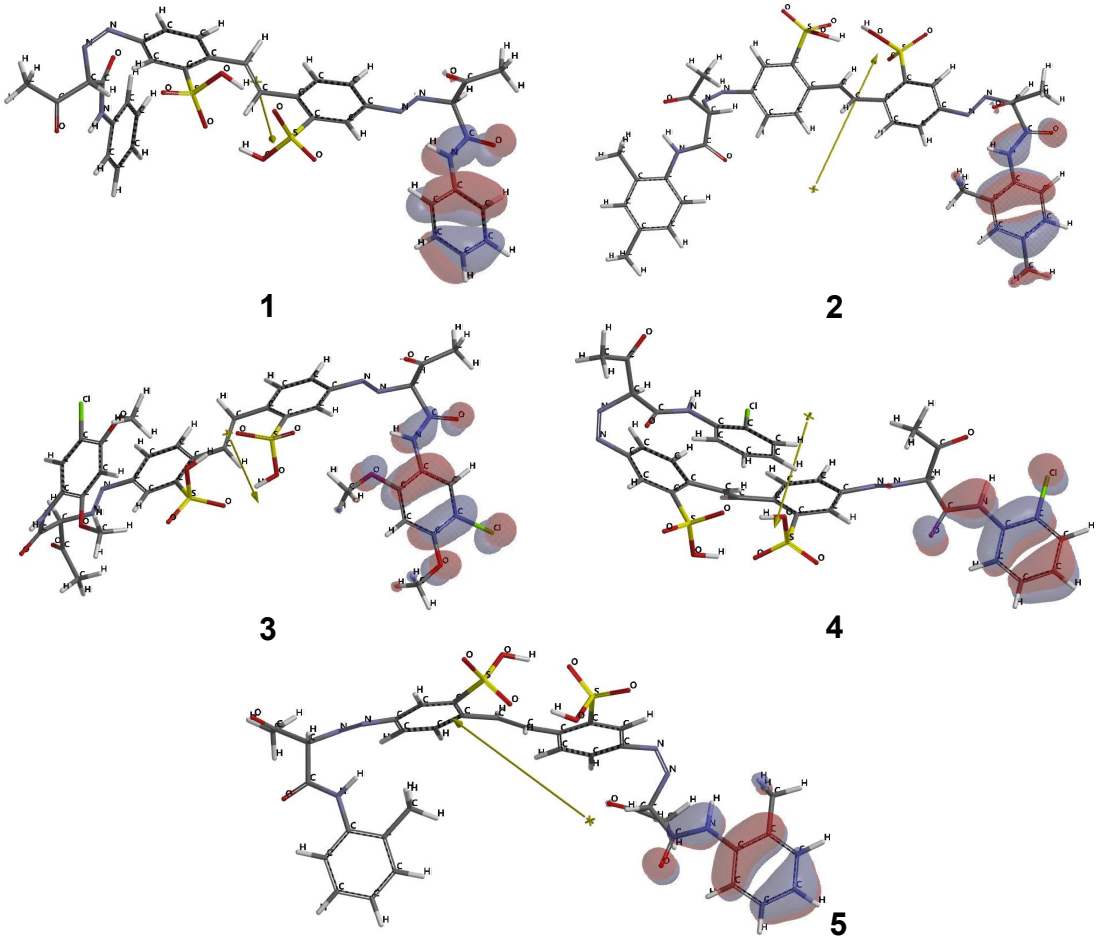

Fig.6 HOMO profiles and dipole moment orientations calculated for the optimized geometries at the ground state for dyes **1** - **5**

Variation of the FO energy thresholds as a result of altering the substituents attached to the acetamidic nitrogen is another argument that upholds the hypothesis that anodic oxidation occurs primarily on the latter site.

Table 3 Frontier orbital energies derived from voltammetric data, calculated dipole moments for dyes **1**-**5**

Dye	E_{onset}^{Ox} /$V_{Fc/Fc+}$	E_{onset}^{Red} /$V_{Fc/Fc+}$	$E_{HOMO/LUMO}$ [a] /eV	Dipole moment[b] /D	E_g [c] /eV
1	0.447	-1.671	-5.55/-3.43	6.25	2.12
2	0.402	-1.777	-5.50/-3.32	7.93	2.18
3	0.418	-1.938	-5.52/-3.16	3.17	2.36
4	0.554	-1.639	-5.65/-3.46	6.11	2.19
5	0.543	-1.639	-5.64/-3.46	8.79	2.18

[a] Estimated using Eq. (5) and (6) respectively

[b] Calculated using DFT methods

[c] Calculated as $E_g = |E_{HOMO}\text{-}E_{LUMO}|$ as estimated from CV [56]

The response of the investigated stilbene derivatives to an externally applied electric field can be quantified by the magnitude and orientation of

the dipole moment obtained through DFT calculations. It is known that molecular dipole moments arise mainly from differences in electronegativity (*i.e.*, charge separation) within the given structure. Higher values of the dipole moment denote a larger charge separation, are hence characteristic for a more polarizable molecule that could adsorb more easily onto the electrode [57]. Data listed in Table 3 suggests that compound **3** (Scheme 1) is the least polarizable substrate while the largest dipole moments are shown by compounds **2** and **5** (Scheme 1), both bearing *methyl* substituents. This behavior is consistent with observations suggesting the strong adsorption tendency of dye **2** as well as an important contribution of the methyl group on molecular dipoles due to its mesomeric electron releasing effect [58].

In our case, the dipole moment seems to correlate well with the electronic effects of the attached functional groups. This means that the electron-donating *methoxy* group accounts for a larger delocalization of spin densities whereas the attached chlorine compensates the latter by its electron attracting inductive effect, leading to lower intramolecular charge separation, as well as for a less positive oxidation potential.

FO energies as well as the so-called HOMO - LUMO gap (E_g), have been calculated and are presented in Fig.7. E_g can be seen as a measure of the energy needed to promote an electron from the molecular HOMO to the LUMO, which is a key step in electron transfer processes. Differences in FO

energies are best quantified by the global hardness (η) or softness (σ) of a molecule (Eq. 11) [59], while molecules exhibiting a large energy difference being considered as hard. Higher orbital energies of the HOMO indicate that the molecule has a more pronounced tendency to donate an electron to an appropriate acceptor, whereas a lower LUMO energy denotes a higher probability for the substrate to accept a negative charge [60]. Thus, a small E_g indicates that a molecule is more likely to undergo electronic transitions and take part in chemical reactions involving electron transfer. Conversely, a larger value of E_g is mostly characteristic for lower reactivity and thus more pronounced kinetic stability of the given molecule [61]. As can be seen in Fig.7, HOMO energies vary within an extremely narrow window ranging from -5.50 eV for compound **3** to -6.33 eV corresponding to substrate **4**. DFT analysis reveals that E_g of the investigated dyes converges following the sequence **3** < **2** < **5** < **1** < **4**, indicating that dye **4** would be the most kinetically stable compound [60], exhibiting an E_g value of 3.43 eV whereas substrate **3**, with the narrowest E_g of 2.35 eV would show higher reactivity [62]. The two, electron releasing *methoxy* substituents, grafted on the outer benzene ring of substrate **3** (Scheme 1) account for an extended conjugation and thus a smaller energy difference [63]. The data obtained experimentally from CV measurements (Table 3) follows the same trend.

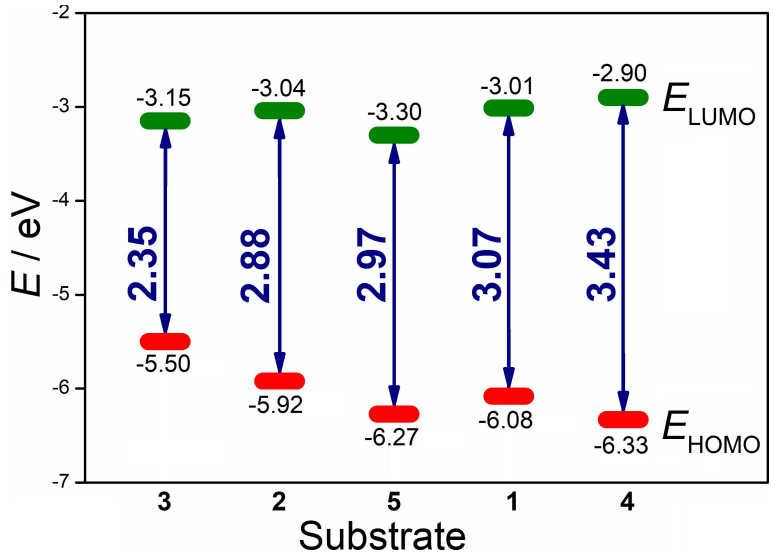

Fig.7 Computed frontier orbital energies and E_g values for substrates **1-5**

Considering all the above data and analyzing the position of the delocalized HOMO orbitals, we can conclude that the investigated substrates undergo an irreversible anodic oxidation, the process being under diffusion control up to sweep rates of 0.1 $V \cdot s^{-1}$. At higher scan rates, surface phenomena start playing a role, since greater overpotentials are needed for substrate oxidation. Finally, the delocalization of the HOMO orbital over the amidic nitrogen atom leads to the assumption that the mechanism could consist of a first slow one-electron charge transfer step with the formation of a radical cation intermediate. The latter could then undergo a subsequent homogenous reaction, most probably deprotonation, thus forming a neutral radical that could go through a second charge transfer forming the final

product, hence following an ECE mechanism, as described by the literature for aromatic amides (Scheme 1) [64, 65].

Scheme 3

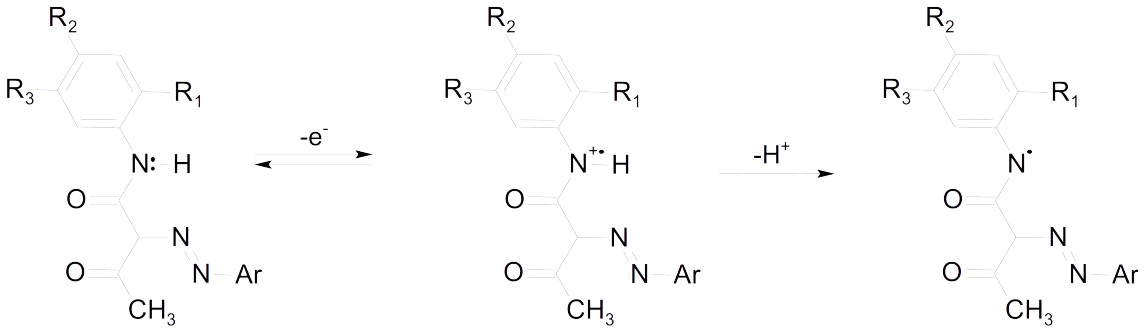

Global reactivity descriptors.

Several computational parameters have been proposed to assess the charge releasing or accepting capacity of a given substrate [66, 67]. One descriptor that correlates the most with the molecular susceptibility to undergoing such types of redox processes is the so-called electrophilicity index ω [68, 69]. The latter parameter which, alongside absolute electronegativity (χ), chemical potential (μ), η or σ, is one of the global reactivity descriptors used in conceptual density functional theory, was firstly defined by Parr et al [66]. It is mainly referred to as a quantification of the energy decrease of a chemical structure due to an optimal electron flux amidst donor and acceptor sites, *i.e.*, the capacity of that structure to act as an electrophile. The operational definition of ω is:

$$\omega = \mu^2/2\eta \qquad (7)$$

Pearson referred to χ and η of a given molecule and outlined their operational descriptions as being dependent on ionization potential (*IP*) and electron affinity (*EA*) as follows [70]:

$$\chi = (IP + EA)/2 = -\mu \quad (8)$$

$$\eta = (IP - EA)/2 \quad (9)$$

Considering Koopmans' theorem as well as subsequent theoretical approaches [71], we can proceed by considering the following relationships to be valid: $E_{HOMO} = -IP$ and $E_{LUMO} = -EA$, thus, obtaining the following expressions as functions of molecular FO energies:

$$\mu = (E_{HOMO} + E_{LUMO})/2 \quad (10)$$

$$\eta = (E_{LUMO} - E_{HOMO})/2 \quad (11)$$

$$\sigma = (1/2)\eta \quad (12)$$

By rearranging the terms, the following expression for the electrophilicity index is obtained:

$$\omega = (E_{HOMO} + E_{LUMO})^2 / 4(E_{LUMO} - E_{HOMO}) \quad (13)$$

The ability of a given substrate of being an electron donor can be quantified by the electrodonating power (ω^-), defined as [67]:

$$\omega^- = (3IP + EA)^2 / 16(IP - EA) \quad (14)$$

Note that a smaller value of ω^- reflects a better electron releasing capacity of the studied substrate [72]. We can thus calculate the above-

mentioned descriptors using the previously DFT computed FO energies; the data for all studied substrates are listed in Table 4.

Table 4. Calculated global reactivity descriptors for the investigated azo dyes.

Global descriptors	Dye				
/ eV	**1**	**2**	**3**	**4**	**5**
IP	6.080	5.920	5.500	6.330	6.270
EA	3.010	3.040	3.150	2.900	3.300
μ	-4.545	-4.480	-4.325	-4.615	-4.785
χ	4.545	4.480	4.325	4.615	4.785
η	1.535	1.440	1.175	1.715	1.485
σ	0.326	0.347	0.426	0.292	0.337
ω	6.729	6.969	7.960	6.209	7.709
ω^-	9,193	9,389	10.269	8.731	10.287

As can be concluded from Table 4, dyes **2** and **3** (Scheme 1) show the smallest *IP*, meaning that these substrates have the most pronounced tendency to donate electrons, being the most easily oxidizable. Considering the *IP* of Pt having a value of 8.959 eV, one can assume that negative charges

from the dyes are more easily transferred towards Pt as the value for *IP* diminishes [73].

A greater value of the electrophilicity index implies a higher stabilization of the molecule due to electronic charge transfer towards it [68, 74], *i.e.*, it is more likely that the molecule is acting more like an electrophile. As data in Table 4 suggests, compounds **3** and **5** (Scheme 1) having the highest electrophilicity index, are stabilized by electron acceptance while substrate **4**, with the smallest electrophilicity index within the series, exhibits the lowest tendency to accept negative charges. The global hardness, η follows the same trend, dye **3** being the least hard molecule of the series.

As expected, the lowest value of the electrodonating power has been computed for substrate **4**, containing a Cl atom grafted on the benzene ring, followed, in order, by the parent compound **1**, followed in order by dyes **2**, **3** and finally **5** with the benzene ring substituted with a methyl group. This behavior closely follows the trend outlined by the variation of the HOMO energies substantiates the role of the substituents grafted on the outer benzene ring, sustaining our assumption, that anodic oxidation affects the amidic nitrogen.

4. Conclusions

The electrochemical behavior of five newly synthesized azostilbene dyes, each having different substituents grafted on the outer benzene rings, has been investigated. The electrochemical measurements conducted in anhydrous DMSO at Pt electrodes indicate that all investigated compounds undergo an irreversible one electron anodic oxidation. It was found that up to sweep rates of 0.1 $V \cdot s^{-1}$, the process is under diffusion control, while at higher scan rates, higher overpotentials are needed for substrate oxidation, most probably due to surface phenomena. The resulting values for anodic transfer coefficients confirm that one electron per substrate molecule is exchanged in the first oxidation step of all studied dyes. The gathered data suggest that the investigated dyes follow an ECE mechanism involving a slow, first one-electron charge transfer step with the formation of a radical cation intermediate, most probably at the amidic nitrogen atom, followed by the deprotonation of the latter and subsequently by a second charge transfer step. DFT computations show that substrates **3** and **5** are the most stabilized by electron acceptance, while the highest ability to donate negative charges is predicted for compounds **4**, **1** and **2** respectively. Further investigations and more detailed quantum chemical calculations are needed to fully elucidate the anodic oxidation of the latter substrates, with the aim of developing new

and environmentally sustainable electrochemical methods for the abatement of dyes from used, or industrial wastewater.

Experimental

Chemicals

The chromogens, derivatives of 4,4'-diaminostilbene-2,2'-disulphonic acid **1** - **5** investigated herein were obtained according to the procedure outlined in the literature [15] and their purity was confirmed by comparing their IR spectra with data detailed earlier [15]. IR determinations have been performed on a Bruker Tensor 37 spectrometer and the results are in close correspondence with those mentioned in literature [15].

Electrochemical investigations

The electrochemical behavior of the stilbene dyes **1** - **5** has been investigated by recording cyclic voltammograms in nonaqueous media over the potential range of interest. Voltammetry measurements were performed in anhydrous, deoxygenated dimethylsulfoxide (DMSO) (Sigma Aldrich) containing 10^{-1} mol·dm^{-3} tetra - *n*- butylammonium tetrafluoroborate (Merck) using an Autolab potentiostat / galvanostat model PGSTAT128N. Data was collected and processed with the Metrohm Nova electrochemistry software. A three-electrode setup was employed consisting of a Pt - disk working electrode (*d* =

3mm), a Pt-wire counter electrode and an Ag/AgCl reference, using a custom-made single compartment cell holding a volume of 7 cm^3 of analyte.

All electrochemical data was gathered at room temperature. The substrate concentration was $2 \cdot 10^{-3}$ $mol \cdot dm^{-3}$. Atmospheric oxygen was removed from solutions by purging N_2 (dried over molecular sieves) before performing the measurements. Solutions were kept under a N_2 layer throughout the experiments to avoid oxygen contamination. Potential values have been referred to the Ferrocene/Ferrocinium (Fc/Fc^+) redox couple used as internal reference as per the IUPAC recommendations [75], unless stated otherwise.

Computational studies

Molecular geometries of the studied substrates have been optimized in the gas phase through quantum chemical calculations using the Spartan'20 software package [76], by performing an initial conformational search using the semi empirical PM6 Hamiltonian computation [77] followed by further pre-optimization using the Hartee-Fock method and the 3-21G basis set in vacuum. Finally, equilibrium geometries of the pre-optimized lowest energy conformers, frontier orbital energies, as well as values and orientation of dipole moments have been computed using the dispersion corrected Becke, 3-parameter, Lee–Yang–Parr (B3LYP-D3) [78-81] density functional method with the 6-31G* basis set in vacuum.

Acknowledgements

The authors would like to thank the International Office at the Vienna University of Technology for contributing to this research though the programme "Mitteln zur Förderung von Auslandsbeziehungen" as well as Univ. Prof. Dipl.-Ing. Dr. Marko Mihovilovic at the Faculty of Technical Chemistry at the Vienna University of Technology for facilitating this research.

References

1. Gürses A, Açıkyıldız M, Güneş K, Gürses MS (2016) Classification of Dye and Pigments. In: Dyes Pigm.. SpringerBriefs in Molecular Science. Springer, Cham., pp 31-45. DOI: https://doi.org/10.1007/978-3-319-33892-7_3

2. Lipskikh OI, Korotkova EI, Khristunova YP, Barek J, Kratochvil B (2018) Electrochim Acta 260:974-985 DOI: https://doi.org/10.1016/j.electacta.2017.12.027

3. Smith RE (2000) Azine Dyes. In: Kirk-Othmer Encyclopedia of Chemical Technology. John Wiley & Sons, pp 1 - 11. DOI: https://doi.org/10.1002/0471238961.0126091419130920.a01

4. Benkhaya S, M'Rabet S, El Harfi A (2020) Heliyon 6 (1):e03271. DOI: https://doi.org/10.1016/j.heliyon.2020.e03271

5. Gester R, Torres A, Bistafa C, Araújo RS, da Silva TA, Manzoni V (2020) Mater Lett. 280:128535. DOI: https://doi.org/10.1016/j.matlet.2020.128535

6. Harisha S, Keshavayya J, Kumara Swamy BE, Viswanath CC (2017) Dyes Pigm. 136:742-753. DOI: https://doi.org/10.1016/j.dyepig.2016.09.004

7. Vázquez-Ortega F, Lagunes I, Trigos Á (2020) Dyes Pigm. 176. DOI: https://doi.org/10.1016/j.dyepig.2020.108248

8. Waheeb AS, Al-Adilee KJ (2021) Mater. Today: Proc. 42:2150-2163. DOI: https://doi.org/10.1016/j.matpr.2020.12.299

9. Zhang H, Wang J, Xie K, Pei L, Hou A (2020) Dyes Pigm. 174. DOI: https://doi.org/10.1016/j.dyepig.2019.108079

10. Song DH, Yoo HY, Kim JP (2007) Dyes Pigm. 75 (3):727-731. DOI: https://doi.org/10.1016/j.dyepig.2006.07.025

11. Halliday SM, Lackman-Smith C, Bader JP, Rice WG, Clanton DJ, Zalkow LH, Buckheit RW, Jr. (1996) Antiviral Res 33 (1):41-53. DOI: https://doi.org/10.1016/s0166-3542(96)00994-1

12. Chao YC, Yang SS (1995) Dyes Pigm. 29 (2):131-138. DOI: https://doi.org/10.1016/0143-7208(95)00038-h

13. Ko C-W, Tao Y-T, Danel A, Krzemińska L, Tomasik P (2001) Chem. Mater. 13 (7):2441-2446. DOI: https://doi.org/10.1021/cm010199u

14. Sekar N (2013) UV-absorbent, antimicrobial, water-repellent and other types of functional dye for technical textile applications. In: Advances in the Dyeing and Finishing of Technical Textiles. pp 47-77. DOI: https://doi.org/10.1533/9780857097613.1.47

15. Grad ME, Raditoiu V, Wagner L, Raditoiu A, Lupea AX (2007) Rev. Chim. 58 (8): 786-790

16. Ravi BN, Keshavayya J, Mallikarjuna NM, Santhosh HM (2020) Chem. Data Collect. 25. DOI: https://doi.org/10.1016/j.cdc.2019.100334

17. Yan M, Kawamata Y, Baran PS (2018) Angew Chem Int Ed. Engl. 57 (16): 4149-4155. DOI: https://doi.org/10.1002/anie.201707584

18. Kaya SI, Cetinkaya A, Ozkan SA (2021) Food Chem Toxicol 156: 112524. DOI: https://doi.org/10.1016/j.fct.2021.112524

19. Heard DM, Lennox AJJ (2020) Angew Chem Int Ed. Engl. 59 (43): 18866-18884. DOI: https://doi.org/10.1002/anie.202005745

20. Nidheesh PV, Zhou M, Oturan MA (2018) Chemosphere 197: 210-227. DOI: https://doi.org/10.1016/j.chemosphere.2017.12.195

21. Pacheco-Álvarez MOA, Picos A, Pérez-Segura T, Peralta-Hernández JM (2019) J. Electroanal. Chem. 838: 195-203. DOI: https://doi.org/10.1016/j.jelechem.2019.03.004

22. Pointer Malpass GR, de Jesus Motheo A (2021) Curr. Opin. Electrochem. 27. DOI: https://doi.org/10.1016/j.coelec.2021.100689

23. Guidelli R, Compton RG, Feliu JM, Gileadi E, Lipkowski J, Schmickler W, Trasatti S (2014) Pure Appl. Chem. 86 (2): 245-258. DOI: https://doi.org/10.1515/pac-2014-5026

24. Costea LV, Bica K, Fafilek G, Mihovilovic MD (2018) Monatsh. Chem. 149 (4): 823-831. DOI: https://doi.org/10.1007/s00706-018-2154-6

25. Costea L-V, Fafilek G, Kronberger H (2014) Environ Eng Manag J. 13 (8):1987-1995. DOI: https://doi.org/10.30638/eemj.2014.220

26. Cui MH, Liu WZ, Tang ZE, Cui D (2021) Water Res. 203:117512. DOI: https://doi.org/10.1016/j.watres.2021.117512

27. Asenjo-Pascual J, Salmeron-Sanchez I, Mauleón P, Agirre M, Lopes AC, Zugazua O, Sánchez-Díez E, Avilés-Moreno JR, Ocón P (2023). J. Power Sources 564:10. DOI: https://doi.org/ARTN 232817 10.1016/j.jpowsour.2023.232817

28. Abad N, Hajji M, Ramli Y, Belkhiria M, Moftah H. Elmgirhi S, A. Habib M, Guerfel T, T. Mague J, Essassi EM (2020). J. Phys. Org. Chem. 33 (6):33:e4055. DOI: https://doi.org/10.1002/poc.4055

29. Tang Y, He D, Guo Y, Qu W, Shang J, Zhou L, Pan R, Dong W (2020). Chemosphere 258:127368. DOI: https://doi.org/10.1016/j.chemosphere.2020.127368

30. Foster RJ, Keyes TE (2007) Behavior of Ultramicroelectrodes. In: Zoski CG (ed) Handbook of Electrochemistry. Elsevier, Amsterdam, Boston, pp 155-260. DOI: https://doi.org/10.1016/b978-0-444-51958-0.X5000-9
31. Scholz F, Bond AM, Compton RG, Fiedler DA, Inzelt G, Kahlert H, Komorsky-Lovrić Š, Lohse H, Lovrić M, Marken F, Neudeck A, Retter U, Scholz F, Stojek Z (2010) Electroanalytical Methods. 2 edn. Springer, Berlin, Heidelberg. https://doi.org/10.1007/978-3-642-02915-8
32. Abbar JC, Meti MD, Nandibewoor ST (2017). Z Phys Chem. 231 (5):957-970. DOI: https://doi.org/10.1515/zpch-2015-0745
33. Bard AJ, Faulkner LR (2001) Electrochemical Methods: Fundamentals and Applications. 2 edn. John Wiley & Sons,
34. Inzelt G (2010) Kinetics of Electrochemical Reactions. In: Scholz F (ed) Electroanalytical Methods. 2 edn. Springer, Berlin, Heidelberg, pp 33-56. DOI: https://doi.org/https://doi.org/10.1007/978-3-642-02915-8
35. Marken F, Neudeck A, Bond AM (2010) Cyclic Voltammetry. In: Scholz F (ed) Electroanalytical Methods. 2 edn. Springer, Berlin, Heidelberg, pp 57-106. DOI: https://doi.org/https://doi.org/10.1007/978-3-642-02915-8
36. Bard AJ, Faulkner LR (2001) Polrarography and Pulse Voltammetry. In: Bard AJ, Faulkner LR (eds) Electrochemical Methods: Fundamentals and Applications. 2 edn. John Wiley & Sons, pp 261-304

37. Masek A, Chrzescijanska E, Zaborski M (2013). Electrochim. Acta 107:441-447. DOI: https://doi.org/10.1016/j.electacta.2013.06.037

38. Al Owais AA, El-Hallag IS (2019). Chem. Pap. 73 (9):2353-2362. DOI: https://doi.org/10.1007/s11696-019-00788-9

39. Gosser DK (1993) Cyclic voltammetry : simulation and analysis of reaction mechanisms. New York (N.Y.) : VCH,

40. Brett CMA, Oliveira Brett AM (1994) Electrochemistry - Principles, Methods and Applications. Oxford University Press, New York

41. Peltola E, Sainio S, Holt KB, Palomaki T, Koskinen J, Laurila T (2018). Anal Chem 90 (2):1408-1416. DOI: https://doi.org/10.1021/acs.analchem.7b04793

42. Arshad N, Ikramullah, Aamir M, Sher M (2016). Monatsh. Chem. 148 (2):245-255. DOI: https://doi.org/10.1007/s00706-016-1768-9

43. Sanecki P, Skital P (2002). Comput Chem 26 (4):297-311. DOI: https://doi.org/10.1016/s0097-8485(01)00123-1

44. Khairy M, Mahmoud BG, Banks CE (2018). Sens. Actuators B Chem. 259:142-154. DOI: https://doi.org/10.1016/j.snb.2017.12.054

45. Nicholson RS, Shain I (1964). Anal Chem 36 (4):706-723. DOI: https://doi.org/DOI 10.1021/ac60210a007

46. Shabik MF, Begum H, Rahman MM, Marwani HM, Hasnat MA (2020). Chem Asian J 15 (24):4327-4338. DOI: https://doi.org/10.1002/asia.202001016

47. Batchelor-McAuley C, Katelhon E, Barnes EO, Compton RG, Laborda E, Molina A (2015). ChemistryOpen 4 (3):224-260. DOI: https://doi.org/10.1002/open.201500042

48. Compton RG, Laborda E, Ward KR (2014) Understanding Voltammetry: Simulation of Electrode Processes. ICP, London. https://doi.org/10.1142/p910

49. Pournaghi-Azar MH, Razmi-Nerbin H (2000). J. Electroanal. Chem. 488 (1):17-24. DOI: https://doi.org/10.1016/s0022-0728(00)00171-6

50. Wang Y, Wu B, Gao Y, Tang Y, Lu T, Xing W, Liu C (2009). J. Power Sources 192 (2):372-375. DOI: https://doi.org/10.1016/j.jpowsour.2009.03.029

51. Sauro VA, Magri DC, Pitters JL, Workentin MS (2010). Electrochim. Acta 55 (20):5584-5591. DOI: https://doi.org/10.1016/j.electacta.2010.04.080

52. Bouchet LM, Peñéñory AB, Robert M, Argüello JE (2015). RSC Adv. 5 (16):11753-11760. DOI: https://doi.org/10.1039/c4ra16154h

53. Adeniyi AA, Ngake TL, Conradie J (2020). Electroanalysis 32 (12):2659-2668. DOI: https://doi.org/10.1002/elan.202060163

54. Cardona CM, Li W, Kaifer AE, Stockdale D, Bazan GC (2011). Adv Mater 23 (20):2367-2371. DOI: https://doi.org/10.1002/adma.201004554

55. Aj Torriero A (2019). Medicinal & Analyt. Chem. Int. J. 3 (4). DOI: https://doi.org/10.23880/macij-16000151

56. Chiu KY, Ha Tran TT, Chang SH, Yang T-F, Su YO (2017). Dyes Pigm. 146:512-519. DOI: https://doi.org/10.1016/j.dyepig.2017.07.049

57. Ghanavatkar CW, Mishra VR, Sekar N, Mathew E, Thomas SS, Joe IH (2020). J. Mol. Struct. 1203:127401-127413. DOI: https://doi.org/10.1016/j.molstruc.2019.127401

58. Salvatella L (2017). Educ. Quím. 28 (4):232-237. DOI: https://doi.org/10.1016/j.eq.2017.06.004

59. Matada MN, Jathi K, Malingappa P, Pushpavathi I (2020). Chem. Data Collect. 25. DOI: https://doi.org/10.1016/j.cdc.2019.100314

60. Mohan A K, Purushothaman A, Janardanan D, Haridas KR (2022). J. Mol. Struct. 1249. DOI: https://doi.org/10.1016/j.molstruc.2021.131621

61. Wang H, Wang X, Wang H, Wang L, Liu A (2007). J Mol Model 13 (1):147-153. DOI: https://doi.org/10.1007/s00894-006-0135-x

62. Aihara J-i (1999). J. Phys. Chem. A 103 (37):7487-7495. DOI: https://doi.org/10.1021/jp990092i

63. Manjunatha B, Bodke YD, Sandeep KJR, Lohith NT, Sridhar AM (2021). J. Mol. Struct. 1244:130933-130942. DOI: https://doi.org/10.1016/j.molstruc.2021.130933

64. Golub T, Becker JY (2012). Org Biomol Chem 10 (19):3906-3912. DOI: https://doi.org/10.1039/c2ob06878h

65. Gieshoff T, Kehl A, Schollmeyer D, Moeller KD, Waldvogel SR (2017). J Am Chem Soc 139 (35):12317-12324. DOI: https://doi.org/10.1021/jacs.7b07488

66. Parr RG, Von Szentpaly L, Liu SB (1999). J Am Chem Soc. 121 (9):1922-1924. DOI: https://doi.org/DOI 10.1021/ja983494x

67. Chattaraj PK, Chakraborty A, Giri S (2009). J Phys Chem A 113 (37):10068-10074. DOI: https://doi.org/10.1021/jp904674x

68. Bhide R, Jadhav AG, Sekar N (2017). Fibers Polym. 17 (3):349-357. DOI: https://doi.org/10.1007/s12221-016-5717-3

69. Mishra VR, Sekar N (2017). J Fluoresc 27 (3):1101-1108. DOI: https://doi.org/10.1007/s10895-017-2045-y

70. Pearson RG (1986). Proc Natl Acad Sci U S A 83 (22):8440-8441. DOI: https://doi.org/10.1073/pnas.83.22.8440

71. Tsuneda T, Song JW, Suzuki S, Hirao K (2010). J Chem Phys 133 (17):174101. DOI: https://doi.org/10.1063/1.3491272

72. Martinez-Gonzalez E, Frontana C (2014). J Org Chem 79 (3):1131-1137. DOI: https://doi.org/10.1021/jo402565t

73. Sanchez-Marquez J, Garcia V, Zorrilla D, Fernandez M (2020). J Phys Chem A 124 (23):4700-4711. DOI: https://doi.org/10.1021/acs.jpca.0c01342

74. Ghanavatkar CW, Mishra VR, Sekar N (2020). Spectrochim Acta A Mol Biomol Spectrosc 230:118064. DOI: https://doi.org/10.1016/j.saa.2020.118064

75. Gritzner G, Kuta J (1984). Pure Appl. Chem. 56 (4):461-466. DOI: https://doi.org/10.1351/pac198456040461

76. Spartan'20 (2021). 1.1.4 edn. Wavefunction Inc., Irvine CA

77. Stewart JJ (2007). J Mol Model 13 (12):1173-1213. DOI: https://doi.org/10.1007/s00894-007-0233-4

78. Becke AD (1993). J. Chem. Phys. 98 (7):5648-5652. DOI: https://doi.org/10.1063/1.464913

79. Lee C, Yang W, Parr RG (1988). Phys Rev B Condens Matter 37 (2):785-789. DOI: https://doi.org/10.1103/physrevb.37.785

80. Grimme S, Antony J, Ehrlich S, Krieg H (2010). J. Chem. Phys. 132 (15):154104-154119. DOI: https://doi.org/10.1063/1.3382344

81. Grimme S, Ehrlich S, Goerigk L (2011). J. Comput. Chem. 32:1456-1465. DOI: https://doi.org/10.1002/jcc.21759

1

Figure Captions

Fig. 1 Cyclic voltammograms of compounds **1** - **5**. Conditions: substrate concentration, c=2·10^{-3} mol·dm^{-3}; scan rate 50·10^{-3} V·s^{-1}. Dotted line: Cyclic voltammogram of **1** - **5** cathodic scan, recorded in the same conditions. Inset: variation of oxidation peak potential with logarithm of scan rate.

Fig. 2 Cyclic voltammogram of **1** over the entire potential window, 4 cycles. Conditions: substrate concentration, c=2·10^{-3} mol·dm^{-3}; v = 50·10^{-3} V·s^{-1}. Inset: variation of oxidation peak height on square root of the scan rate.

Fig. 3 Cyclic voltammogram of **1**, anodic region. Conditions: substrate concentration, c=2·10^{-3} mol·dm^{-3}; scan rates 10 - 400·10^{-3} V·s^{-1} Inset A: Plot of log$I$ vs. log$v$ for the oxidation peak of substrate **1**. Inset B: Variation of the current function ($I_A \cdot v^{-1/2}$) with v for the oxidation peak of substrate **1**

Fig. 4. Cyclic voltammogram of **2** anodic region. Conditions: substrate concentration, c=2·10^{-3} mol·dm^{-3}; scan rates 0.01 - 0.4· V·s^{-1} Inset: Variation of the current function ($I_A \cdot v^{-1/2}$) with v for the oxidation peak of substrate **2**

Fig. 5 Variation of E_A-$E_{A/2}$ on the scan rate range 0.01-0.4 $V \cdot s^{-1}$ for compounds **1** - **5**. Inset: *Tafel* plot drawn from the rising part of the current-potential curve of compound **1** recorded at $v = 0.01$ V s^{-1}

Fig.6 HOMO profiles and dipole moment orientations calculated for the optimized geometries at the ground state for dyes **1** - **5**

Fig.7 Computed frontier orbital energies and E_g values for substrates **1-5**

Table 1 Voltammetric data collected for dyes **1** - **5**[a)]

Dye	E_A / V[b)]	E_{C1} / V	E_{C2} / V	E_{C3} / V	$(E_A$-$E_{A/2}) \cdot 10^{-3}$/ V	$(\partial E_A/\partial \log v)$ / V
1.	0.696	-0.988	-1.579	-1.742	0.179	0.076
2.	0.491	-1.678	-1.791	--	0.099	0.061
3.	0.749	-0.989	-1.788	-2.136	0.205	0.199
4.	0,677	-0.956	-1.499	-1.727	0.157	0.097
5.	0.725	-0.960	-1.466	-1.778	0.156	0.139

[a)] Conditions: substrate concentration $c=2 \cdot 10^{-3}$ mol·dm^{-3}; $v = 50 \cdot 10^{-3}$ $V \cdot s^{-1}$

[b)] Potentials referred to the Fc/Fc^+ redox couple

Table 2. Anodic transfer coefficient, assumed number of electrons, mean value of ΔE_p

Dye[a)]	α_{rd}[b)]	α_{avg}[c)]	α_{app}[d)]	*n'* (assumed)	$(E_A\text{-}E_{A/2})_{avg}$/ V
1	0.308	0.388	0.283	1	0.199
2	0.276	0.401	0.478	1	0.101
3	0.265	0.188	0.249	1	0.205
4	0.349	0.304	0.332	1	0.167
5	0.366	0.293	0.326	1	0.168

[a)]Conditions: substrate concentration $c=2\cdot10^{-3}$ mol·dm^{-3}, ref. Ag/AgCl

[b)] Data obtained from the *Tafel* plot at $v = 0.01$ V·s^{-1}

[c)] Data obtained from the slope of E_A vs. log$v$; up to $v = 0.1$ V·s^{-1}

[d)] Data obtained using Eq. (4)

Table 3 Frontier orbital energies derived from voltammetric data, calculated dipole moments for dyes **1**-**5**

Dye	E_{onset}^{Ox} /$V_{Fc/Fc+}$	E_{onset}^{Red} /$V_{Fc/Fc+}$	$E_{HOMO/LUMO}$[a)] /eV	Dipole moment[b)] /D	E_g[c)] /eV
1	0.447	-1.671	-5.55/-3.43	6.25	2.12
2	0.402	-1.777	-5.50/-3.32	7.93	2.18
3	0.418	-1.938	-5.52/-3.16	3.17	2.36
4	0.554	-1.639	-5.65/-3.46	6.11	2.19
5	0.543	-1.639	-5.64/-3.46	8.79	2.18

[a)] Estimated using Eq. (5) and (6) respectively

[b)] Calculated using DFT simulations

[c)] Calculated as $E_g = |E_{HOMO}-E_{LUMO}|$ as estimated from CV [56]

Table 4. Calculated global reactivity descriptors for the investigated azo dyes.

Global descriptors	Dye				
/ eV	**1**	**2**	**3**	**4**	**5**
IP	6.080	5.920	5.500	6.330	6.270
EA	3.010	3.040	3.150	2.900	3.300
μ	-4.545	-4.480	-4.325	-4.615	-4.785
χ	4.545	4.480	4.325	4.615	4.785
η	1.535	1.440	1.175	1.715	1.485
σ	0.326	0.347	0.426	0.292	0.337
ω	6.729	6.969	7.960	6.209	7.709
ω^-	9,193	9,389	10.269	8.731	10.287

1 *Figure 1*

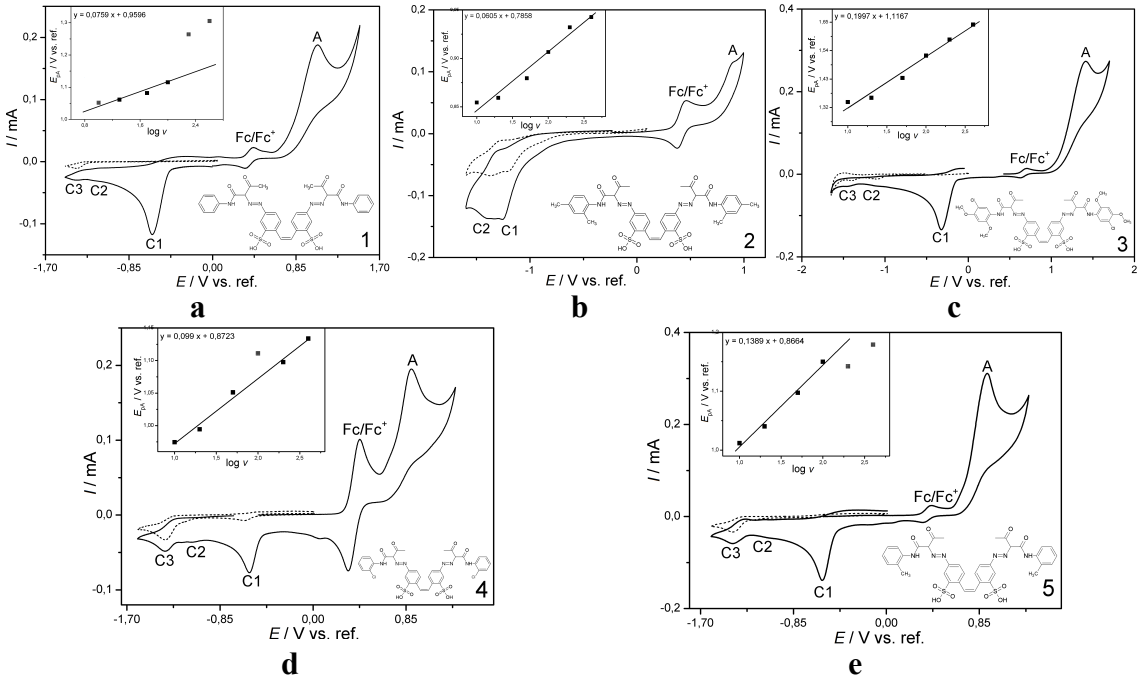

2

3 *Figure 2*

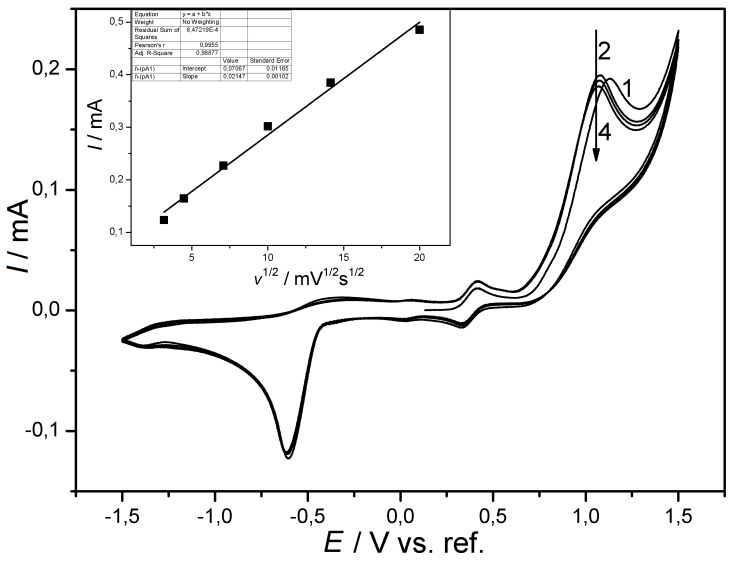

4

5

6

7

1 *Figure 3*

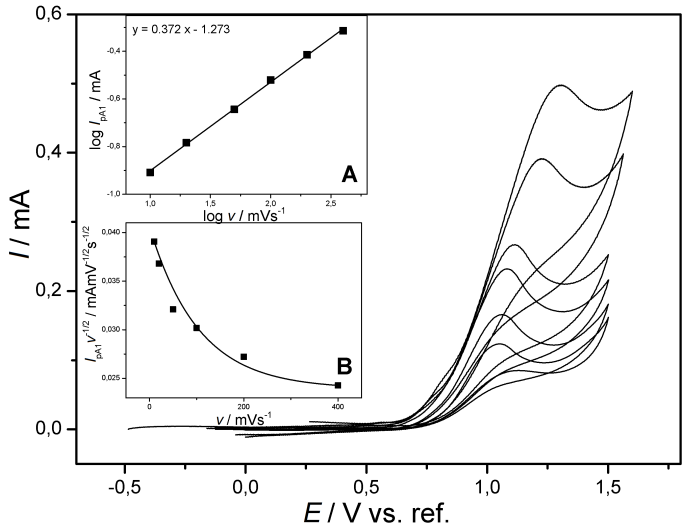

2

3

4 *Figure 4*

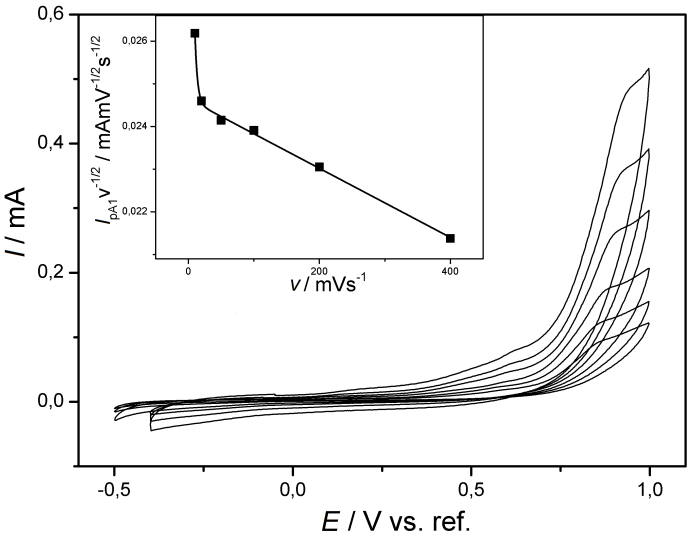

5

6

7 *Figure 5*

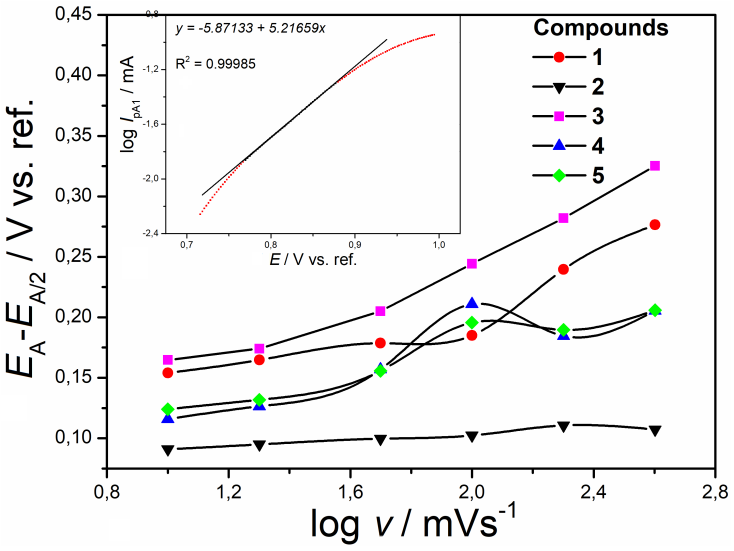
y = -5.87133 + 5.21659x
R² = 0.99985
log I_{pA1} / mA
E / V vs. ref.
Compounds
1
2
3
4
5
E_A-$E_{A/2}$ / V vs. ref.
log v / mVs^{-1}

Figure 6

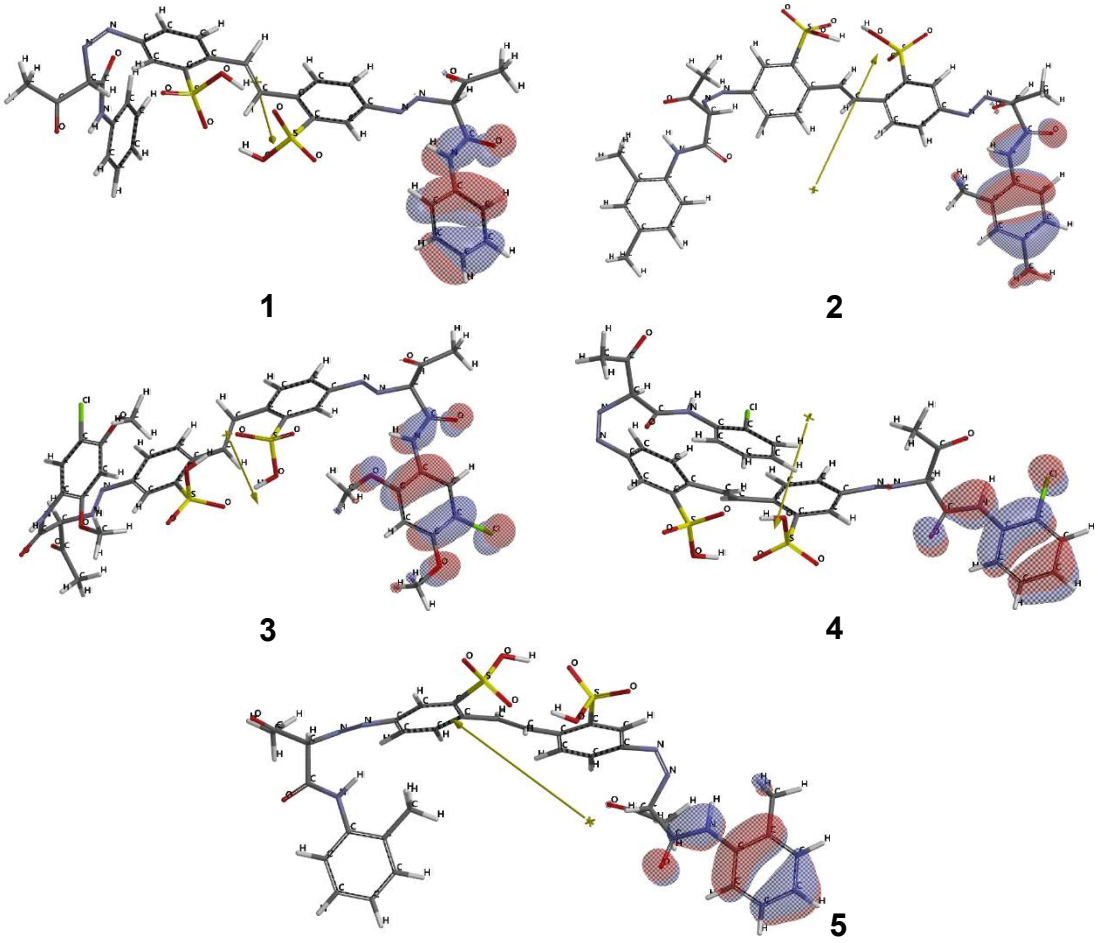
1
2
3
4
5

Figure 7

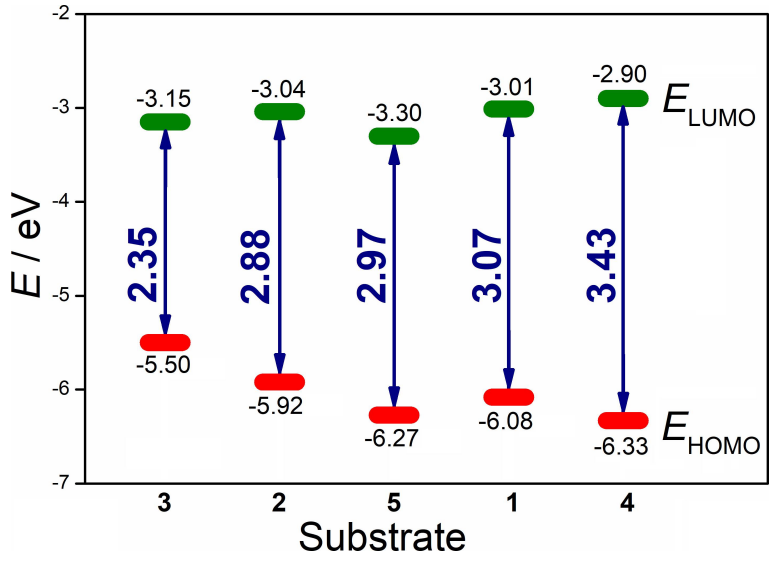

Scheme 1

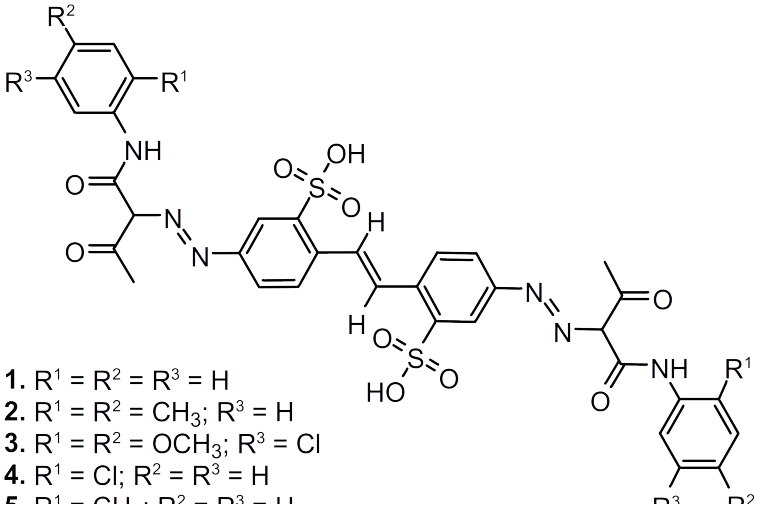

1 *Scheme 2*

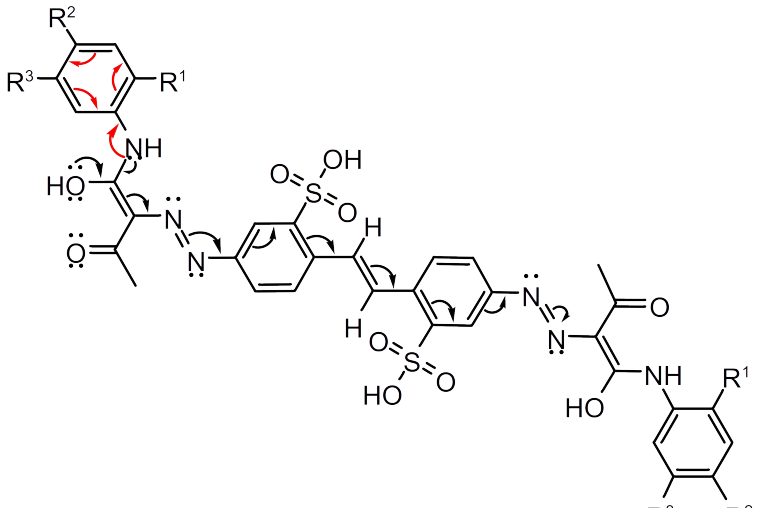

2

3 *Scheme 3*

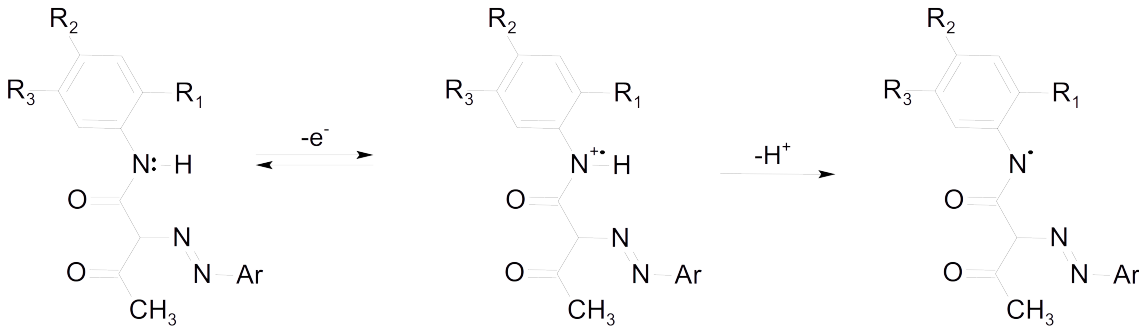

4

Graphical abstract